

Effect of Heat Input on Mechanical and Metallurgical Properties of Friction Stir Welded AA6061-10% SiCp MMCs

P. Periyasamy, B. Mohan, and V. Balasubramanian

(Submitted August 22, 2011; in revised form November 22, 2011)

Metal matrix composites (MMCs) reinforced with SiC particles combine the matrix properties with those of the ceramic reinforcement, leading to higher stiffness and superior thermal stability with respect to the corresponding unreinforced alloys. However, their wide application as structural material needs proper development of a suitable joining process. In this investigation, an attempt was made to study the effect of heat input on the evolution of microstructure in weld region of friction stir welded AA6061-10% SiCp MMCs. The tensile properties of the joints were evaluated and they are related with microstructure and heat input of the process. The microstructure characterization of the weld zone shows evidence of a substantial grain refinement of the aluminum matrix and fracturing of reinforcement particles due to dynamic recrystallization induced by the plastic deformation and frictional heating during welding.

Keywords friction stir welding, metal matrix composites, microstructure, tensile properties

1. Introduction

Metal matrix composites (MMCs) are very attractive materials, due to their high stiffness (high strength and modulus with low density), high temperature stability, and superior wear resistance, compared to the unreinforced alloys (Ref 1-4). However, despite the large amount of scientific papers on their microstructural and mechanical characterization, at present MMCs have not reached widespread industrial application. The reasons for this are several, the major ones being the production costs and also the problems related to the secondary manufacturing processes, such as cutting, machining, forming, and joining (Ref 5-7). These problems are less important, but not absent, in the case of particle reinforced aluminum-based composites, the most widely studied among MMCs. With regard to the joining processes, it seems that all processes that can be used to join aluminum alloys can also be applied to join Al-based MMCs. However, a number of difficulties have been identified, mainly in the case of fusion welding techniques. The problems are linked to: high viscosity of MMCs melt above the melting point, if compared with the unreinforced alloy; segregation of the reinforcement during resolidification; rein-

forcement-matrix interactions; and evolution of the occluded gases (Ref 8). In recent years, a new solid-state joining technique, the friction stir welding (FSW) process, has been successfully applied to several aluminum alloys, leading to joint properties (such as strength, toughness, fatigue life) in some cases higher than those of the base material (Ref 9-15). A detailed description of the FSW process is present in the literature (Ref 16-18).

The mechanical properties of cast A319 Al alloy was improved by FSW because of the reduction in the size of second phase particles, uniform distribution of Si particles, and reduction of percentage porosity volume (Ref 13). Kim et al. (Ref 19) observed that the size of the Si particles in the bottom is smaller than that in the top or the middle, while the size in the retreating side is almost the same as that on the advancing side. The Si particle size decreases with the increasing welding speed. However, it is not significantly affected by the rotation speed.

The previous papers related to FSW of MMC have focused on microstructure characteristics of the welds. The weld nugget exhibits the relatively homogeneous SiCp distributions but has fine particle density bands. In addition, the nugget contains some porosity around the coarse SiCp and cracking of some coarse SiCp. The TMAZ, which is adjacent to the weld nugget, which has been plastically deformed and thermally affected (Ref 20). Statistical experiments were performed to identify the significant variables and their effects on the hardness, tensile and bending strength, ductility, and microstructure of the weld by using A356/SiC/15p AlSiC MMC (Ref 21). The abrasive effect of the tool pin on the ceramic reinforcement led to reduction of the particles size, but no reduction in the particles shape-factor. The hardness in the nugget was compared with base metal and it was found that it was slightly increased in TMAZ (Ref 22). Homogeneous distribution of SiCp as well as spheroidization of silicon needles and their spreading through the matrix were the dominant reasons for property improvement in the stir zone. Band-like arrangement of SiCp and silicon

P. Periyasamy, Department of Mechanical Engineering, St. Peter's Engineering College, Chennai 600054, Tamil Nadu, India; **B. Mohan**, Department of Production Technology, MIT, Anna University, Chennai 600044, Tamil Nadu, India; and **V. Balasubramanian**, Department of Manufacturing Engineering, Centre for Materials Joining & Research (CEMAJOR), Annamalai University, Annamalainagar 608002, Tamil Nadu, India. Contact e-mails: psamy75@gmail.com, mohan@mitindia.edu, and visvabalu@yahoo.com.

needles leads to an increase in the hardness of the transitional zone in comparison with the base composite (Ref 23).

However, the investigations on FSW of cast aluminum MMCs are limited, and most of the reported literature on the FSW of aluminum with Al_2O_3 p, SiCp, and Ti-based MMCs were carried out on A359/AA6061/AA2024 grade aluminum alloy. In all these above works, the effect of process parameters such as tool rotational speed, welding speed, axial force, tool shoulder diameter, and tool pin profile on mechanical and metallurgical properties were studied individually but there is no literature available on the effect of frictional heat generation and its effect on joint properties.

Hence, an attempt was made to understand the effect of heat input of FSW process on the evolution of microstructure in weld zone of AA6061-10% SiCp MMCs. The tensile properties of the joints were evaluated and they are presented in this paper.

2. Experimental

Casting of unmodified AA6061 aluminum alloy matrix, reinforced with 10 vol.% fraction of SiC particles were made by the sand casting method, and they were machined to rectangular plates of 150 mm × 100 mm × 6 mm. The chemical composition and mechanical properties of base metal are presented in Table 1 and 2, respectively. Square butt joint configuration, was prepared to fabricate FSW joints. The initial joint configuration was obtained by securing the plates in position using mechanical clamps. A non-consumable tool made of high speed steel (HSS) tool with a shoulder diameter of 18 mm and a threaded pin of 6 mm diameter, 5.7 mm long, and 1 mm pitch (Fig. 1) was used for welding. An ingeniously designed and developed FSW machine (15 hp; 3000 rpm; 25 kN) was used to fabricate the joints. Five joints were fabricated (Fig. 2) using different heat input conditions and the welding conditions are presented in Table 3. The welded joints were sliced using power hacksaw and then machined to the required dimensions to prepare tensile and microstructure specimens.

Two different tensile specimens were prepared to evaluate the transverse tensile properties. Smooth (unnotched) tensile specimens (Fig. 3b) were prepared to evaluate transverse tensile properties of the joints such as yield strength, tensile strength, elongation, and reduction in cross-sectional area. Notched specimens (Fig. 3c) were evaluated for notch tensile strength and notch strength ratio of the joints. Tensile testing was carried out using a 100 kN, electromechanical controlled

Table 1 Chemical composition (wt.%) of base metal

Al	Mg	Si	Cu	Cr	Fe	Mn	Ti	Zn
97.9	0.92	0.5	0.228	0.219	0.139	0.053	0.002	0.002

Table 2 Mechanical properties of base metal

Yield strength, MPa	Ultimate tensile strength, MPa	Elongation, %	Hardness @ 0.5 kg Hv
200	278	8.0	105

UTM. The images of the specimens before and after the tensile test are shown in Fig. 4. The specimens for microstructure analysis were polished using different grades of emery papers. Final polishing was done using the diamond compound (1 μ m particle size) in the disc-polishing machine. Specimens were etched with Keller's reagent to reveal the microstructure. Microstructural analysis was carried out using a light optical microscope (Make: MEIJI, Japan; Model: MIL-7100) incorporated with an image analyzing software (Metal Vision MVLx1.0). Hardness across the weld was measured with 0.5 kgf load and a dwell period of 15 s using Vickers Microhardness tester. The fractured surface of the tensile specimens was analyzed using a SEM (Make: JEOL, Japan; Model 5610LV) at high magnification to study the fracture morphology to establish the nature of the fracture.

3. Results

3.1 Tensile Properties

The transverse tensile properties, such as yield strength, tensile strength, elongation, reduction in cross-sectional area, and joint efficiency of friction stir welded cast aluminum MMCs joints were evaluated. In each condition, three specimens are tested and the average of three results is calculated and they are presented in Table 4. The load displacement curve of AA6061-10% SiCp MMCs welded joints are displayed in Fig. 5.

From the results, it can be inferred that the heat input has significant influence on tensile properties of the FSW joints of AA6061-10% SiCp MMCs. Of the five joints fabricated, the joint fabricated with the heat input of 1039 J mm⁻¹ exhibited higher yield strength of 126 MPa, tensile strength of 206 MPa, elongation of 6.5%, and the joint efficiency of 74%. Notch strength ratio (NSR) was found to be less than unity irrespective of the welded joints. This suggests that the cast aluminum alloy is sensitive to notches and it comes under the 'notch brittle materials' category. The NSR is 0.90 for unwelded

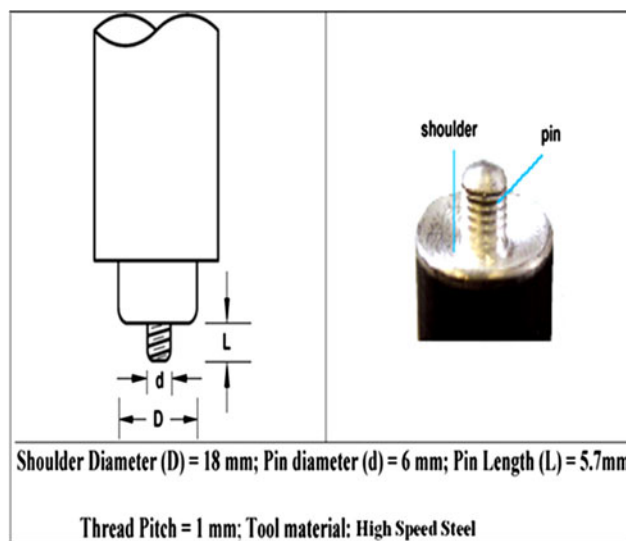


Fig. 1 FSW tool details

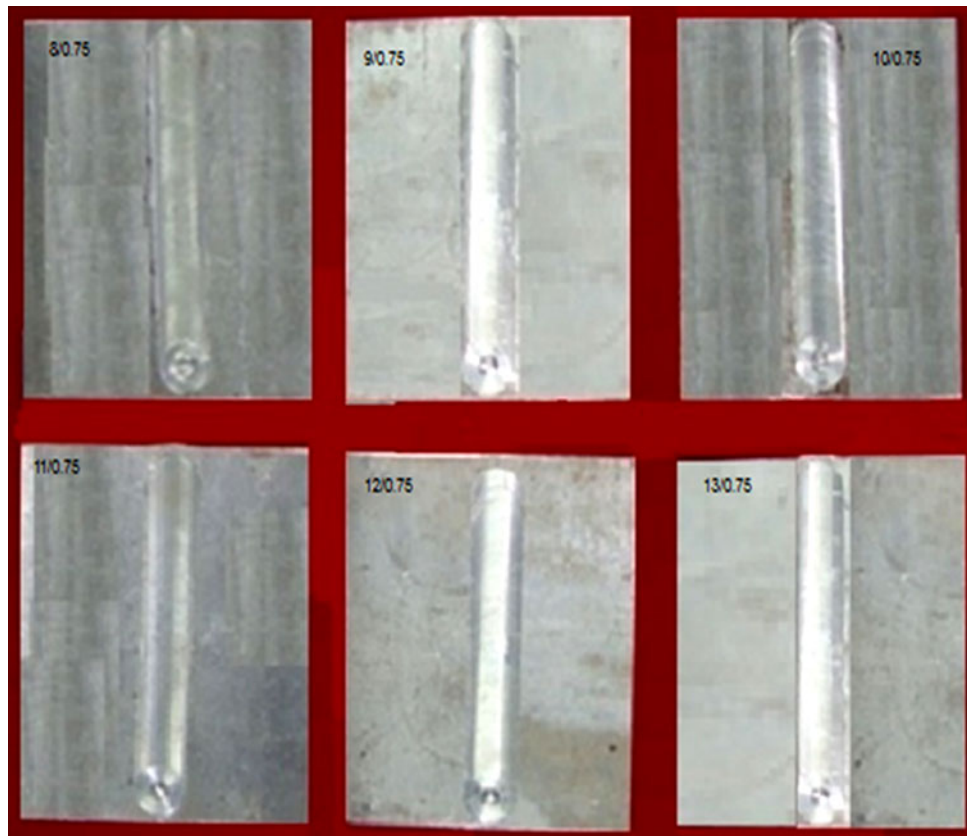


Fig. 2 Fabricated FSW joints

Table 3 Welding conditions used to fabricate the joints

Joint number	Tool rotational speed, rpm	Welding speed, mm min ⁻¹	Axial force, kN	Tool shoulder dia	Heat input, J mm ⁻¹
1	800	45	6	18	755
2	900	45	6	18	850
3	1000	45	6	18	945
4	1100	45	6	18	1039
5	1200	45	6	18	1133

Heat input = $q = (2\pi/3s) \times \mu \times P \times \omega \times R_s \times \eta$ (Ref 28), where s , welding speed in 0.75 mm/s; P , axial force in 6 kN; ω , rotational speed in rev/s; R_s , shoulder radius in 0.009 m; μ , coefficient of friction Al/steel $\mu = 0.47$

parent metal and FSW causes further reduction in NSR of the welded joints. A similar phenomenon was reported (Ref 24).

3.2 Macrostructure Analysis

During FSW, the material flowed around the tool pin due to the heat generated by the friction and stirring action. FSW joints are prone to defects like pinholes, tunnels, cavities, kissing bonds, etc., due to insufficient and excess heat input in the stir zone (Ref 25). All the joints fabricated in this investigation were analyzed at low magnification using optical microscope to reveal the quality of the weld cross-section. The macrographs of the weld nugget region for five levels of heat input are presented in Table 5. Of the five heat input used to fabricate the joints, a heat input of 1039 J mm⁻¹ produced a

defect-free weld. It is also observed that the all the tensile tested specimens invariably failed at weld nugget region.

3.3 Microstructure Analysis

During the tensile test, all the specimens failed away from the weld nugget region (Table 4). Hence, the microstructure analysis was made in the weld nugget and TMAZ region to identify the reasons. The microstructure of base metal (Fig. 6a) consists of SiC particles intermetallic (dendritic) phase of aluminum matrix and elongated grains. Optical micrographs of the nugget region of all the joints are displayed in Fig. 6. Virtually all traces of dendritic solidification microstructure were eliminated throughout the nugget zones and also the SiC particles was uniformly dispersed in the weld nugget because of

the stirring action of the dynamically recrystallized condition of the metal during FSW. This phenomenon was reported by other investigators also (Ref 23).

From the micrographs, it can be observed that there is an appreciable variation in grain size at the weld region with respect to the heat input of the welding process. The joint fabricated with the heat input of 1039 J mm^{-1} contained finer grains compared to the other joints (Fig. 6e).

Figure 7 shows SEM images indicating the size and distribution of SiCp in the weld nugget, which were obtained at different heat input conditions. It was found that the size of the SiCp at the heat input of 1039 J mm^{-1} is smaller than the other heat input conditions. In this condition the SiCp will be finer and more granular due to the solid collisions at the optimum heat input, as a result of the more difficult plastic deformation.

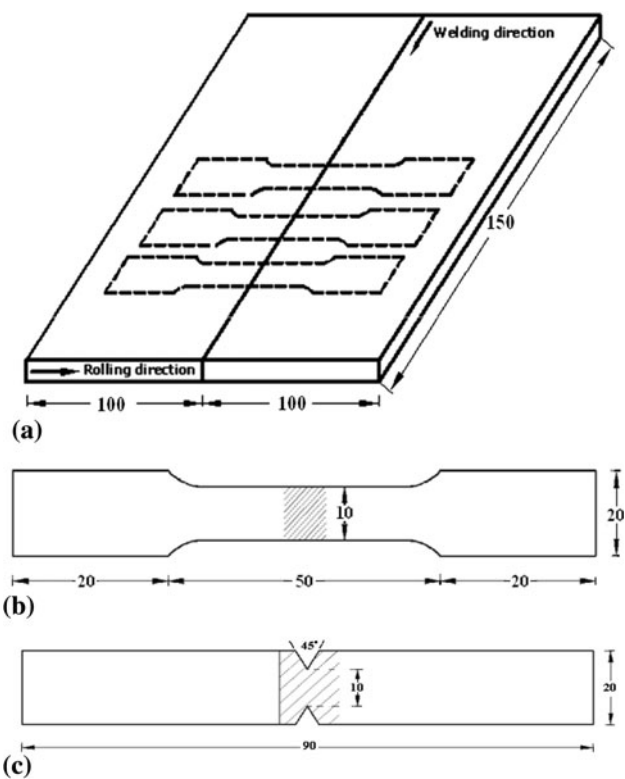


Fig. 3 Dimensions of joint and tensile specimens. (a) Scheme of extraction of tensile specimen. (b) Dimensions of un-notched tensile specimen. (c) Dimensions of notched tensile specimen

3.4 Microhardness Survey

Microhardness was measured at mid-thickness region across the welded joints and the values are presented in Fig. 8. The base metal hardness is 105 Hv. The hardness of the weld nugget is considerably higher than that of the base metal irrespective of the heat input used. The difference in hardness between the heat-affected zone and weld nugget is attributed to the grain refinement in the weld nugget (Ref 25). The joint fabricated with the heat input of 1039 J mm^{-1} recorded the highest hardness values of 95 Hv in the weld nugget region when compared to other joints and this was one of the main reasons for superior tensile properties of this joint. The lowest hardness was recorded in the joint fabricated with the heat input of 755 J mm^{-1} . The hardness of weld nugget is not only influenced by the grain size of the microstructure, it is also affected by the metal flow behavior under the effect of heat input, that decides the amount of work hardening of the metal in the weld nugget. Based on the results, it is considered that the size and distribution of the SiCp affected by the different heat input conditions. The number of finer SiCp, which were formed due to the stirring by the tool probe and heat input, increases during FSW. The size of the SiCp should increase with the increasing heat input. However, the size should decrease with increasing flow rate. Based on the two different effects, the size of the SiCp is not significantly changed by the increasing heat input. Very fine SiCp are more uniformly distributed in the weld nugget region. These suggest that the weld nugget region is more stronger than the other region.

3.5 Fracture Surface Analysis

The fracture surfaces of tensile specimens of friction stir welded cast aluminum alloy were analyzed using SEM to reveal the fracture surface morphology. Figures 9 and 10 display the fractographs of unnotched and notched tensile specimens, respectively. The fractographs invariably consists of dimples, which is an indication that the most of the unnotched specimens failed in ductile manner under the action of tensile loading (Ref 26). Though all the specimens contain dimples at the fracture surface, there is an appreciable variation in size of the dimples. This is mainly because of variation in grain size of weld nugget region caused by different heat input involved during FSW. The joint fabricated at a heat input of 1039 J mm^{-1} contains finer dimples than the other joints.

When viewed on a SEM scale, the fracture surfaces revealed agglomerations of reinforced particles which caused local stress concentrations in the composite and lead to crack formation in the matrix. Presence of hard and brittle SiC particles in the ductile Al matrix exerts constraints on the plastic flow of the matrix. When combined with concentration and triaxiality of

Table 4 Transverse tensile properties of FSW joints

Joint number	Heat input, J mm^{-1}	Yield strength, MPa	Tensile strength, MPa	Elongation, %	Reduction in c.s.a., %	Notch tensile strength, MPa	NSR	Joint efficiency, %
1	755	96	170	5.2	4.0	130	0.76	61
2	850	110	182	5.8	4.7	138	0.79	65
3	945	118	193	6.0	5.0	146	0.82	69
4	1039	126	206	6.5	5.6	162	0.85	74
5	1133	112	190	6.1	5.1	150	0.82	68

Table 5 Effect of heat input of welding process on weld cross-section and location of failure

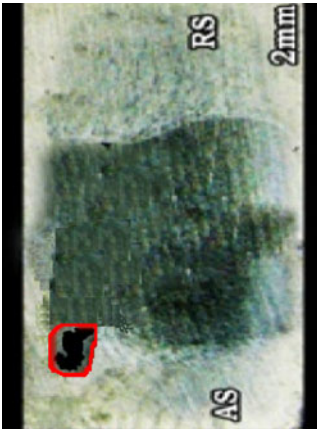



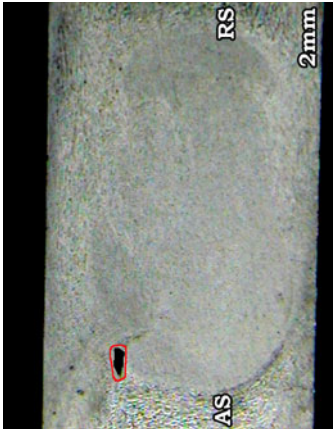

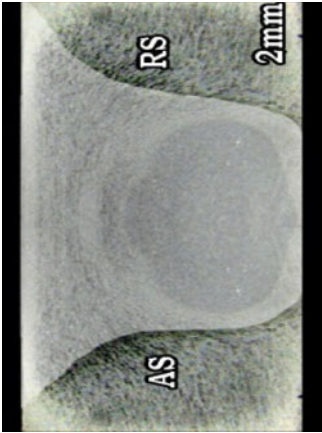

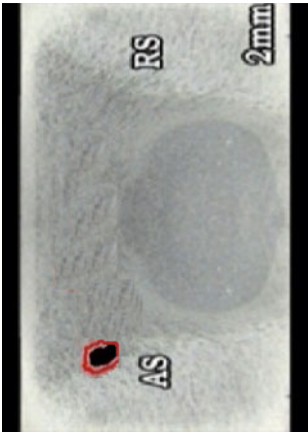

Heat input, $J\ mm^{-1}$	Macrograph of weld cross-section	Observations	Tensile specimen (after testing)	Observations
755		Pin hole defect at the AS of the TMAZ		Fracture in HAZ
850		Worm hole at the AS of the TMAZ		Fracture in TMAZ
945		Worm hole at the AS of the TMAZ		Fracture in TMAZ

Table 5 Continued

Heat input, J mm ⁻¹	Macrograph of weld cross-section	Observations	Tensile specimen (after testing)	Observations
1039		No defect		Fracture in BM
1133		Tunnel defect at the AS of the TMAZ		Fracture in TMAZ

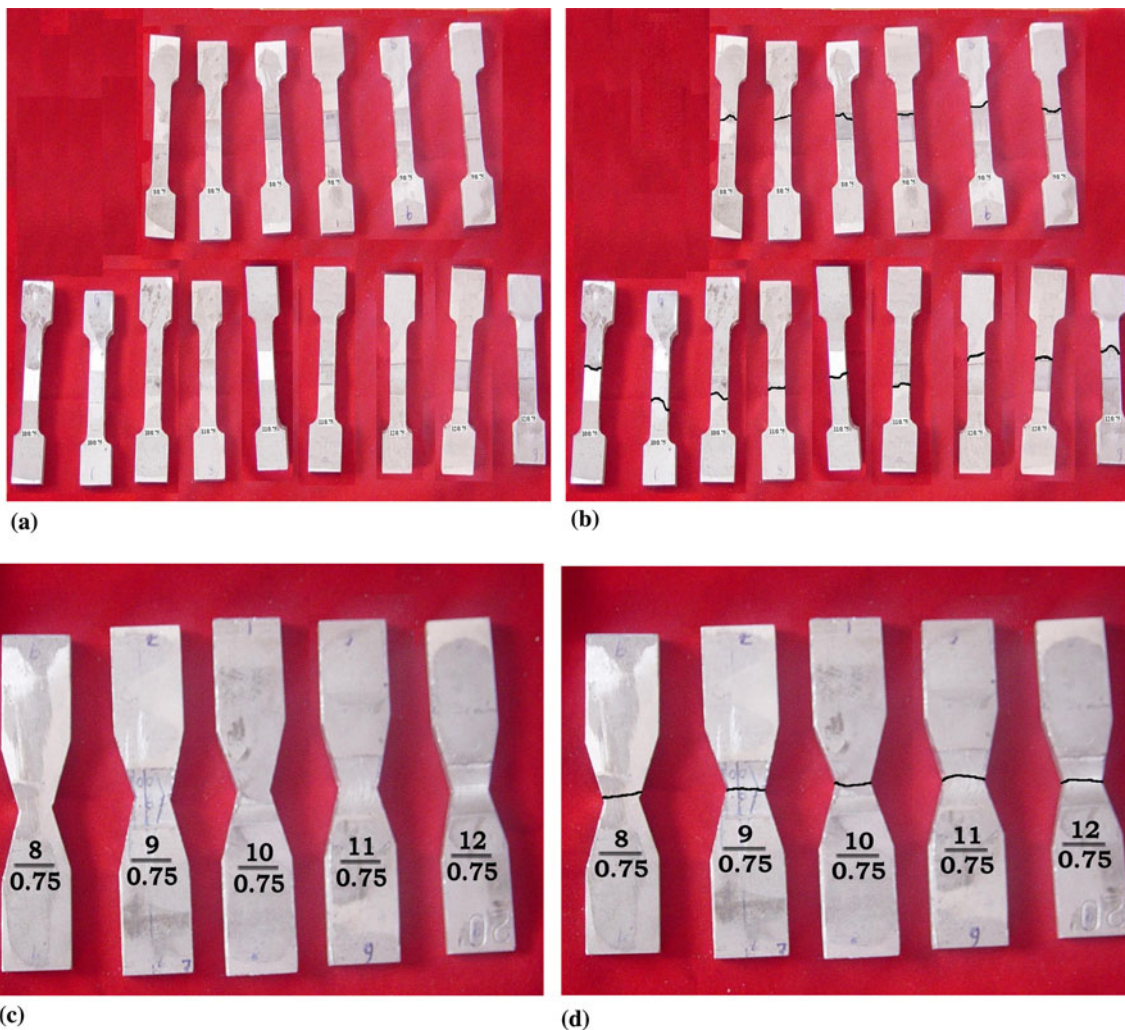


Fig. 4 Photograph of tensile specimens. (a) Unnotched tensile specimen (before testing). (b) Unnotched tensile specimen (after testing). (c) Notch tensile specimen (before testing). (d) Notch tensile specimen (after testing)

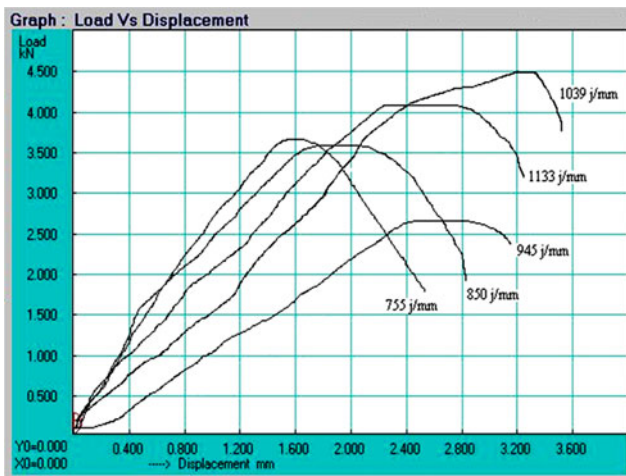


Fig. 5 Effect of heat input of welding process on tensile load vs displacement curves

stress in clustered particles regions, the composite undergoes brittle fracture without showing appreciable ductility. Figures 9 and 10 show the non-uniform direction of reinforcing particles

in the fracture surface of AA6061-10% SiCp MMCs. Some of the particles on the fracture surface are presented. Similar results were obtained by other investigators also (Ref 27).

4. Discussion

Of five joints fabricated using different heat input conditions, the joints fabricated using a heat input of 1039 J mm^{-1} exhibited superior tensile strength and maximum joint efficiency of 74%, due to the formation of fine eutectic SiC particles uniformly distributed in the aluminum matrix and also the absence of defects in the weld zone (Table 5). The joints fabricated at a heat input of $< 1039 \text{ J mm}^{-1}$ consists of coarse SiC particles and clustered structure in the weld nugget (Fig. 6), which in turn, reduces the joint strength. Similarly, the joints fabricated at a high heat input of 1133 J mm^{-1} consists of a tunnel defect at a AS of the TMAZ and consists of coarser SiC particles (Fig. 6). The optimum heat input, uniform distribution of fine SiC particles, and defect-free weld nugget region, are the reasons for the enhancement of joint strength at a optimum heat input of 1039 J mm^{-1} (Fig. 10).

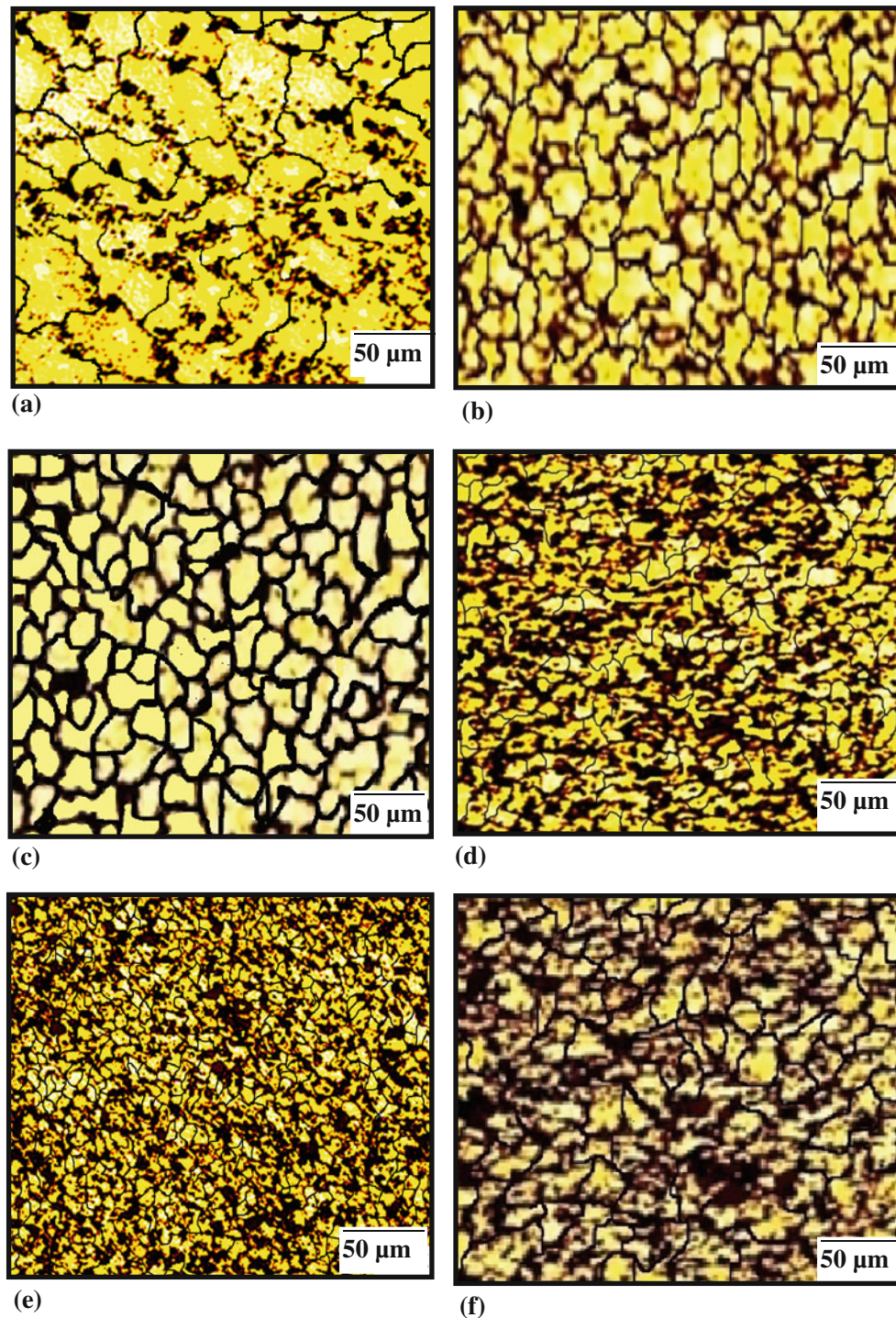


Fig. 6 Optical micrograph of weld nugget region of AA6061 + 10% SiCp MMCs joints. (a) Base metal. (b) 755 J mm⁻¹. (c) 850 J mm⁻¹. (d) 945 J mm⁻¹. (e) 1039 J mm⁻¹. (f) 1133 J mm⁻¹

The heat input (generated by the friction between tool shoulder and base metal) increases with increase in tool rotational speed and decreases with welding speed. Low heat input (<1039 J mm⁻¹) causes the intermittent metal flow and improper stirring action around the tool pin due to insufficient plasticization of the base metal under the tool shoulder. High heat input (>1039 J mm⁻¹) causes the turbulent metal flow around the tool pin due to excess plasticization of base metal under the tool shoulder. Both these welding conditions

produced defective welds (Table 5). Similar results were obtained by other investigators also (Ref 25). In this investigation, the heat input was calculated using the expression proposed by Heuriter et al. (Ref 28) and the heat input values are presented in Table 3. From table, it is understood that the heat input is having directly proportional relationship with the tool rotational speed.

Lower tool rotational speed results in lower heat input (755 J mm⁻¹) and this leads to the lack of stirring due to the

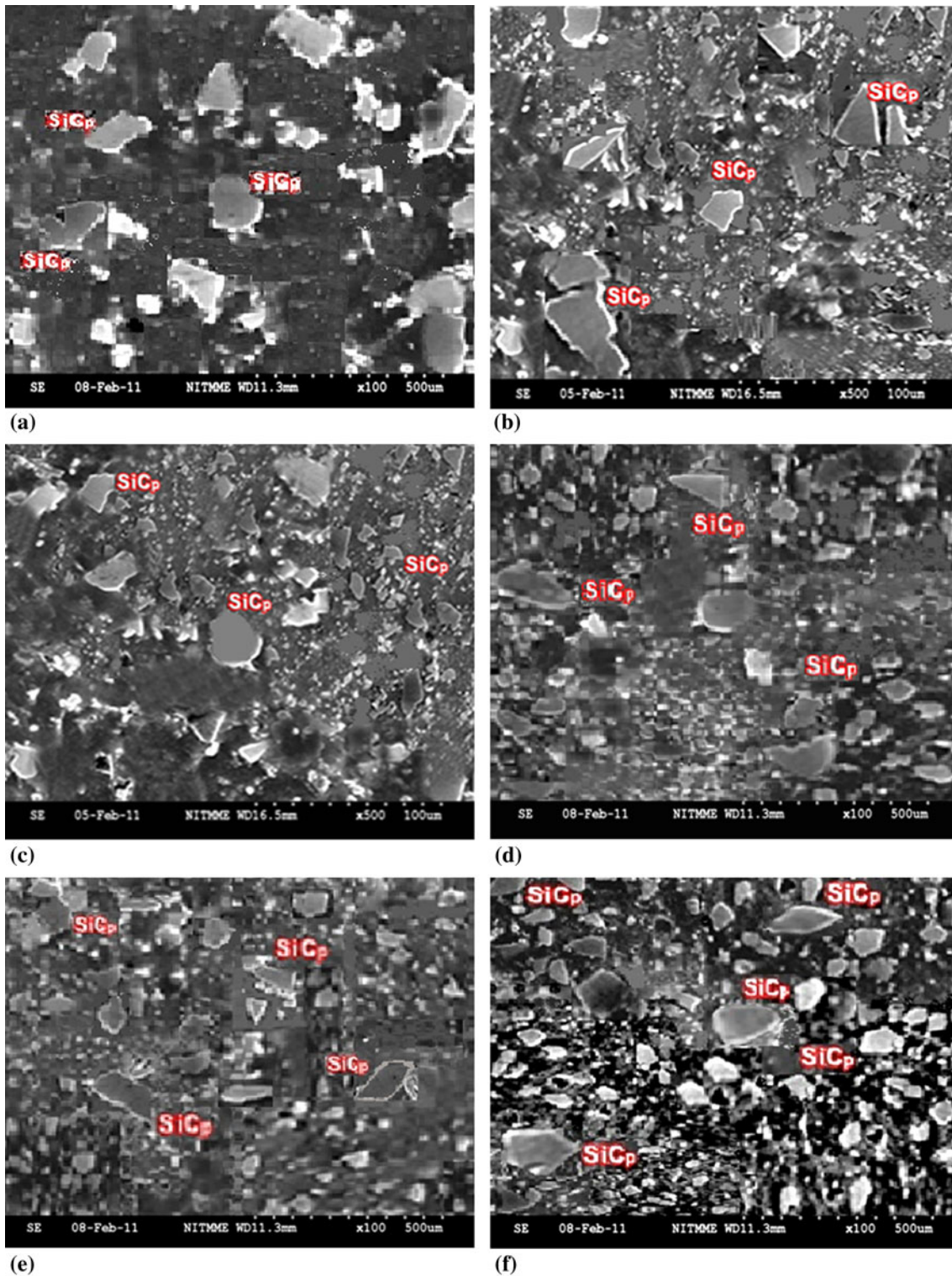


Fig. 7 SEM images of the stir zone of AA6061 + 10% SiCp MMCs joints. (a) Base metal. (b) 755 J mm^{-1} . (c) 850 J mm^{-1} . (d) 945 J mm^{-1} . (e) 1039 J mm^{-1} . (f) 1133 J mm^{-1}

insufficient heat input (Ref 25) which resultantly produces defects (pin hole) in the weld nugget. Moreover, the low heat input causes lower peak temperature and faster cooling rate and this leads to the formation of coarse grains in the weld nugget, which resultantly produced lower hardness in the weld nugget. The lower heat input, the reduction of tensile strength is due to the coarse eutectic SiC particles and non-homogeneous distri-

bution in the matrix. So the combined effect of coarse grains, lower hardness, and presence of defects deteriorated the tensile strength of the joint fabricated using heat input in the range of ($755\text{-}945 \text{ J mm}^{-1}$).

Optimum heat input (1039 J mm^{-1}) leads to sufficient metal flow and adequate plasticization, and leads to defect-free weld nugget. Moreover, the optimum heat input produced very fine

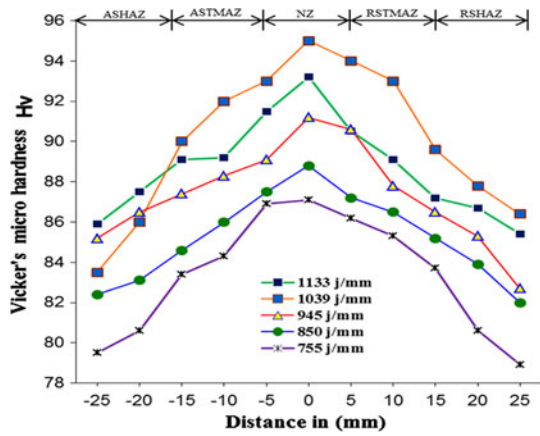


Fig. 8 Effect of heat input of welding process on microhardness profile across the weld region

recrystallized grain structure with uniform distributed precipitates and higher tensile strength is also attributed by the uniform distribution of fine SiC particles in the aluminum matrix of the weld region (Fig. 6e), these are all the reason for higher tensile strength and high hardness of the joint, fabricated under this condition.

Higher tool rotational speed results in higher heat input (1133 J mm^{-1}) and this leads to the excessive release of stirred metal to the upper surface (Ref 25) which resultantly produces defects (tunnel) in the weld nugget. Moreover, the higher heat input causes higher peak temperature and slow cooling rate and this leads to the formation of coarse grains in the weld nugget, which resultantly produced lower hardness in the weld nugget. The higher heat input, the reduction of tensile strength is due to the turbulence of softened metal at high heat input, in which the broken SiC particles are clustered to form coarse particles and segregated (Fig. 6f). So the combined effect of coarse grains,

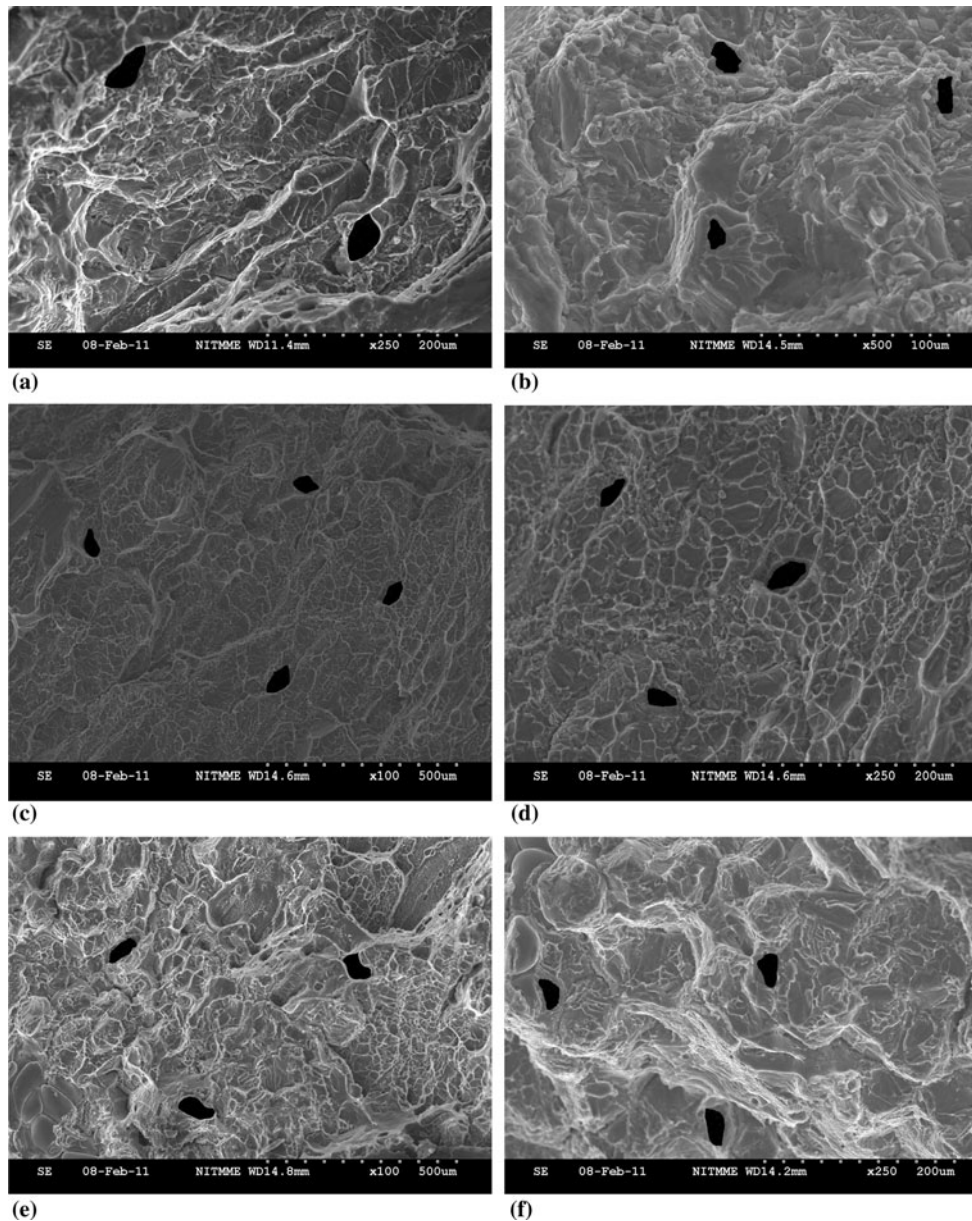


Fig. 9 Effect of heat input of welding process on fracture surface morphology of unnotched tensile specimens. (a) Base metal. (b) 755 J mm^{-1} . (c) 850 J mm^{-1} . (d) 945 J mm^{-1} . (e) 1039 J mm^{-1} . (f) 1133 J mm^{-1}

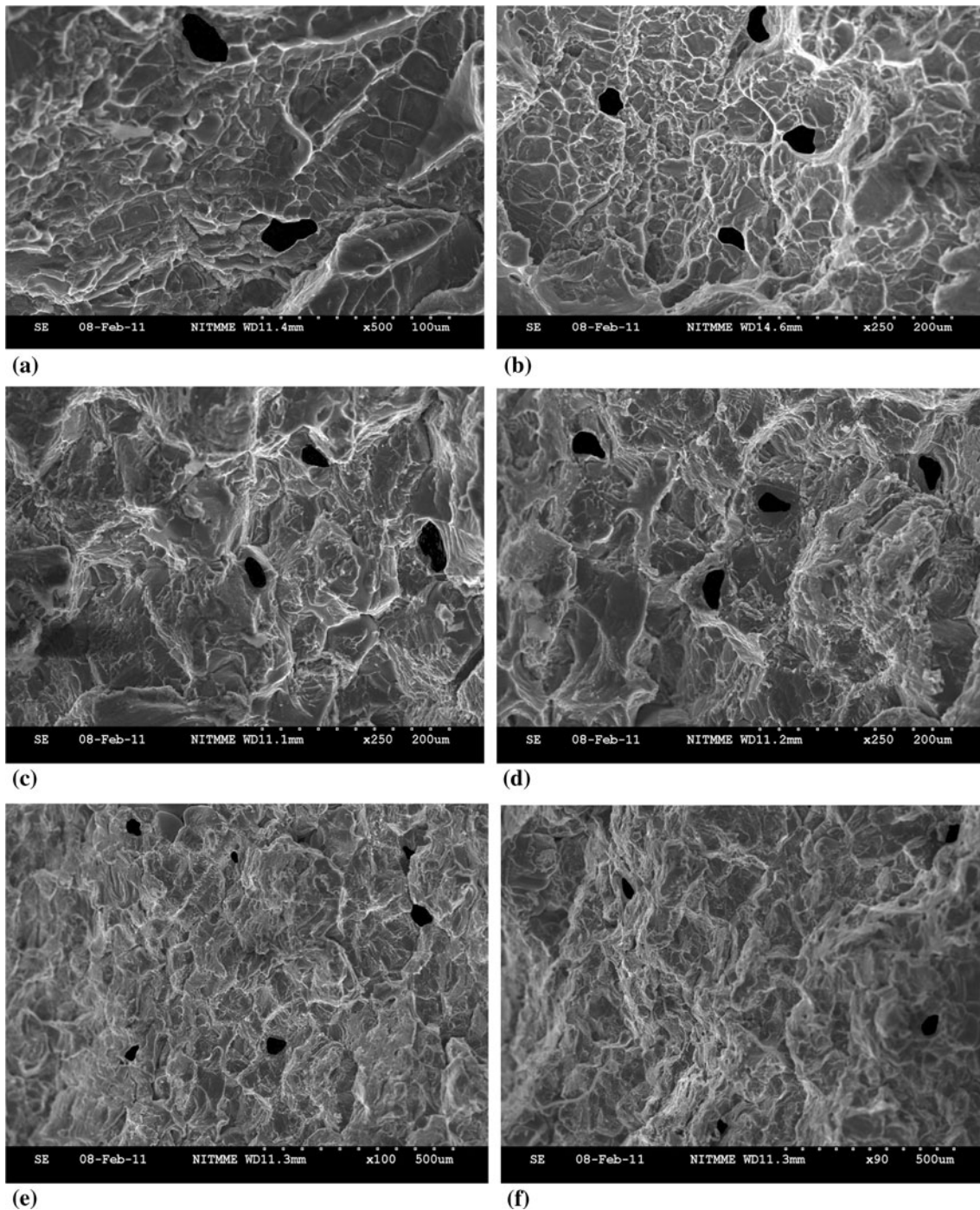


Fig. 10 Effect of heat input of welding process on fracture surface morphology of notched tensile specimens. (a) Base metal. (b) 755 J mm^{-1} . (c) 850 J mm^{-1} . (d) 945 J mm^{-1} . (e) 1039 J mm^{-1} . (f) 1133 J mm^{-1}

lower hardness, and presence of defects deteriorated the tensile strength of the joint fabricated using heat input of (1133 J mm^{-1}).

5. Conclusions

In this article, the effect of heat input on tensile properties, macrostructure, microhardness, microstructure, and fracture

surface of friction welded AA6061-20% SiCp MMCs was analyzed. From this investigation, the following important conclusions are derived:

1. The heat supplied (generated due to friction) during FSW process has significant influence on the macrostructure, microstructure, and microhardness of weld nugget region and subsequently influenced the tensile properties of the joints.
2. Of the five heat input conditions used to fabricate the joints, the joint fabricated using a heat input of 1039

J mm⁻¹ yielded better tensile properties compared to other joints.

- Heat input of 1039 J mm⁻¹ caused free flow, adequate plasticization, and good consolidation of stirred metal at the weld nugget region. This is evident from defect-free, fine-grained, uniform distribution of SiCp, and higher hardened weld nugget region. These are the reasons for better tensile properties of the joint fabricated under this heat input condition.

Acknowledgments

The authors are grateful to the Center for Materials Joining and Research (CEMAJOR), Department of Manufacturing Engineering, Annamalai University, Annamalai Nagar, India, for extending the facilities of Metal Joining and Material Testing to carry out this investigation.

References

- M.A. Kothari, M.S. Thesis, Texas A&M University, 2005, p 1–75
- X. Yong Gan, D. Solomon, and M. Reinbolt, Friction Stir Processing of Particle Reinforced Composite Materials, *Materials*, 2010, **3**(1), p 329–350. doi:10.3390/ma3010329
- C.J. Dawes and W.M. Thomas, Friction Stir Process Welds Aluminum Alloys, *Weld. J.*, 1996, **75**, p 41–45
- J.M. Torralba, C.E. DaCosta, and F. Velasco, P/M Aluminum Matrix Composites: An Overview, *J. Mater. Process. Technol.*, 2003, **5**, p 203–208
- M.W. Mahoney, C.G. Rhodes, J.G. Flintoff, R.A. Spurling, and W.H. Bimgel, Properties of friction-stir-welded 7075 T651 aluminium, *Metall. Mater. Trans. A*, 1998, **29A**, p 1955–1964
- E.D. Nicholas and S.W. Kallee, Causing a Stir in the Future, *Weld. Join.*, 1998, **18**, p 18–21
- E.D. Nicholas, Friction Stir Welding—A Decade On, *IIW Asian Pacific International Congress, Sydney, Australia*, 29 Oct–2 Nov, 2000
- L.E. Murr, G. Liu, and J.C. McClure, A TEM Study of Precipitation and Related Microstructures in Friction-Stir Welded 6061 Aluminum, *J. Mater. Sci.*, 1998, **33**, p 1243–1251
- O.V. Flores, C. Kennedy, L.E. Murr, D. Brown, S. Pappu, B.M. Nowak, and J.C. McClure, Microstructural Issues in a Friction-Stir-Welded Aluminum Alloy, *Scripta Mater.*, 1998, **38**, p 703–708
- T. Hashimoto, S. Jyogan, K. Nakata, Y.G. Kim, and M. Ushio, Flaws in Friction Stir Welds, *Proceedings of the First International Symposium on FSW, 14–16 June, 1999*, Rockwell Science Center, Thousand Oaks, CA, USA
- C.G. Andersson, R.E. Andrews, B.J.I. Dance, M.J. Russel, E.J. Olden, and R.M. Sanderson, Friction Stir Welding of Oxygen Free Cu 60%, 40% Zn and Cu Alloy, *Proceedings of the Second FSW Symposium on Comparison of Copper Canister Fabrication by the Electron Beam and FSP, June 26–28, 2000*, Gothenburg, Sweden
- S.G. Lim, S.S. Kim, C.G. Lee, and S.J. Ki, Tensile Behavior of Friction-Stir-Welded Al 6061-T651, *Metall. Mater. Trans. A*, 2004, **35**, p 2829–2837
- M.L. Santeela, T. Engstrom, D. Storjohann, and T.Y. Pan, Friction Stir Welding of Al MMCs, *Scripta Mater.*, 2005, **53**, p 201–209
- M.P. Miles, B.J. Decker, and T.W. Nelson, Formability and Strength of Friction-Stir-Welded Aluminum Sheets, *Metall. Mater. Trans. A*, 2004, **35**, p 3461–3468
- M.J. Jones, L.P. Heurtier, C. Desrayaud, F. Montheillet, D. Allehaux, and J.H. Driver, Correlation Between Microstructure and Microhardness in a Friction Stir Welded 2024 Aluminium Alloy, *Scripta Mater.*, 2005, **52**(8), p 693–697
- W.M. Thomas, Friction Stir Butt Welding, International Patent Application no. PCT/GB92/02203 and GB Patent Application no. 9125978.8, US Patent no. 5460, 317, Dec 1991
- C. Dawes and W. Thomas, TWI, GB Patent Application no. 9125978.8, US Patent no. 5468, 344, Dec 1991
- M. Ellis and M. Strangwood, Properties of Friction Stir Welded 7075 T651 Aluminium, *TWI Bulletin*, 1995, **6**, p 138–148
- Y.G. Kim, H. Fujii, T. Tsumura, T. Komazaki, and K. Nakata, Effect of Welding Parameters on Microstructure in the Stir Zone of FSW Joints of Al Die Casting Alloy, *Mater. Lett.*, 2006, **60**, p 3830–3837
- H. Uzun, Friction Stir Welding of SiCp Reinforced AA2124 Al Alloy Matrix Composite, *Mater. Des.*, 2007, **28**, p 1440–1446
- M. Amirizad, Evaluation of Microstructure and Mechanical Properties in Friction Stir Welded A356 + 15%SiCp Cast Composite, *Mater. Lett.*, 2006, **60**, p 565–568
- M.A. Kothari, “Welding of Cast A359/SiC/10p MMCs,” Master’s Thesis, Texas A&M University, 1988
- L. Ceschini, I. Boromei, G. Minak, A. Morri, and F. Tarterini, Microstructure, Tensile and Fatigue Properties of AA6061/20vol.%-Al₂O₃p Friction Stir Welded Joints, *Compos. Part A*, 2007, **38**, p 1200–1210
- S. Malarvizhi, K. Raghukantan, and N. Viswanathan, Effect of Post Weld Aging Treatment on Tensile Properties of Electron Beam Welded AA2219 Aluminium Alloy, *Int. J. Adv. Manuf. Technol.*, 2008, **37**, p 294–301
- S. Rajakumar, C. Muralidharan, and V. Balasubramanian, Influence of FSW Process Parameters on Strength Properties of AA7075-T6 Al Alloy Joints, *Mater. Des.*, 2011, **32**, p 535–549
- S. Malarvizhi and V. Balasubramanian, Effect of Welding Processes on AA2219 Aluminium Alloy Joint Properties, *Trans. Non-ferrous Met. Soc. China*, 2011, **21**, p 88–95
- P. Cavaliere, A. Squillace, and F. Panella, Effect of Welding Parameters on Mechanical and Microstructural Properties of AA6082 Joints Produced by Friction Stir Welding, *J. Mater. Technol.*, 2008, **28**, p 364–372
- P. Heurtier, Mechanical and Thermal Modeling of FSW, *J. Mater. Process. Technol.*, 2006, **171**, p 348–357